Journal of Alloys and Compounds 825 (2020) 153982

Contents lists available at ScienceDirect

Journal of Alloys and Compounds

journal homepage: http://www.elsevier.com/locate/jalcom

Impact of post annealing and hydrogen implantation on functional properties of Cu_2O thin films for photovoltaic applications

Raj Kumar*, Kristin Bergum, Heine Nygard Riise, Eduard Monakhov, Augustinas Galeckas, Bengt Gunnar Svensson

Department of Physics, Centre for Materials Science and Nanotechnology (SMN), University of Oslo, P. O. Box 1048 Blindern, 0316, Oslo, Norway

A R T I C L E I N F O

Article history:
Received 25 June 2019
Received in revised form
18 January 2020
Accepted 20 January 2020
Available online 24 January 2020

Keywords:
H^+ doses
Cu_2O
Thin films
Post annealing temperature
Hall effect
Photoluminescence

A B S T R A C T

Polycrystalline cuprous oxide (Cu_2O) thin films were sputtered, annealed (900 °C rapid thermal annealing) and subsequently implanted with various hydrogen ion (H^+) doses from 5E13 to 2E15 cm^{-2} with a low acceleration energy of 36 keV at room temperature to tailor the functional properties of the thin films for solar cell application. The annealed and H^+ implanted Cu_2O thin films were post annealed at low temperatures from 100 °C to 600 °C in an inert atmosphere to promote hydrogen passivation of prevalent intrinsic acceptors and tune the carrier concentration for optimum performance as an absorption layer in a heterojunction solar cell. The H^+ incorporation and post annealing tuned the structural, optical and electrical properties of annealed polycrystalline Cu_2O thin films. The results show an enhancement of the excitonic feature around ~2.0 eV with H^+ dose. The normalized photoluminescence (PL) area around ~1.7 eV was drastically enhanced with increasing H^+ doses compared to excitonic and copper vacancy related area. The normalized total PL quantum efficiency shows an enhancement in yield with elevated H^+ doses by two orders of magnitude. The hole concentration decreases down to ~10^{13} cm^{-3}, while hole mobility and resistivity increase to ~27 cm^2/V and ~2.4 kΩcm, respectively, as the H^+ implantation goes from lower to higher doses. In addition, the post annealing and H^+ incorporation lead to a change in the energy level of the major acceptor from 0.21 eV to 0.27 eV above the valence band maximum. By following the qualitative (PL analysis) and quantitative (Hall data) outcomes, we can conclude that H^+ implantation and post annealing likely indicates the passivation of both acceptor defects and compensating donor defects.

© 2020 The Authors. Published by Elsevier B.V. This is an open access article under the CC BY license (http://creativecommons.org/licenses/by/4.0/).

1. Introduction

Hole transport semiconductor oxide materials have a great potential for sustainable energy conversion device applications (TiO_2/Ga_2O_3/Cu_2O and TiO_2/Al:ZnO/Cu_2O *etc.*) [1]. Cuprous oxide (Cu_2O) with 'intrinsic' p-type conductivity is a non-toxic, low cost, and earth-abundant solar energy material (Cu_2O/SnO_2 heterojunction for solar cell) [2]. Cu_2O has been a subject of extensive research in last few decades [3] due to its high potential as an absorber layer in a tandem hetero junction (Cu_2O/ZnO heterojunction) [4] solar cell structure based on silicon [5]. Cu_2O has also been explored for various applications, e.g. p-type thin film (TF) (ZnO/Cu_2O heterojunction) [6], p-channel Cu_2O thin-film transistors (TFTs)/complementary metal-oxide-semiconductor (CMOS) devices [7], photovoltaic-photo electrochemical cell using p-n Cu_2O TFs and ZnO nanorods [8], polyhedral Cu_2O crystal [9] and Cu_2O TF deposited using glancing angle deposition (GLAD) technique for chemical gas sensors [10], Cu_2O–TiO_2 hybrid nanostructure for biosensor [11]. In addition, Cu_2O was utilized as a transparent conducting layer for monolithic perovskite CIGS tandem solar cells [12], ZnO@Au@Cu_2O nanotube arrays as efficient visible-light-driven photoelectrod [13], flexible-transparent p-n junction of N-doped Cu_2O/SnO_2 on flexible (polyethylene naphthalate) substrate [14], solar cells (ZnO/Cu_2O and/or Cu_2O/ZnO heterojunctions) [15–18]. Moreover, Cu_2O was also exploited in many other energy saving or generating semiconductor devices such as a promising cathode for thermal battery (Li/Cu_2O electrochemical cells) [19], photodetector (ITO/MoS_2/Cu_2O) with ultrahigh sensitivity [20], Cu_2O nanoparticles as a hole-injecting layer with inorganic cesium lead bromide ($CsPbBr_3$) perovskite light emitting diode [21], Cu_2O nanowire photocathodes for water splitting [22], and

* Corresponding author.
E-mail address: raj.kumar@smn.uio.no (R. Kumar).

https://doi.org/10.1016/j.jallcom.2020.153982
0925-8388/© 2020 The Authors. Published by Elsevier B.V. This is an open access article under the CC BY license (http://creativecommons.org/licenses/by/4.0/).

optoelectronic device applications [23].

However, the theoretical efficiency limit of TF based tandem hetero junction solar cell has been estimated ~30% using a top and bottom cell approach, 22% for a material of band gap 1.5 eV and 16% for a material of band gap 2.1 eV [24]. The present maximum experimental efficiency of solar cells based on p-Cu_2O:Na as an absorber combined with n-type $Zn_{1-x}Ge_xO$ is limited to 8.1% [25] due to lack of understanding of intrinsic properties like defects [26] and doping conditions of Cu_2O [27]. Moreover, in recent years, different techniques (e.g. Cd_2SnO_4/CdS/Cu_2O/Ag using chemical technique [28], Ag:Cu_2O nanocomposites by pulsed laser [29]) and approaches (perovskite structure with Cu_2O as a hole-transporting layer for photovoltaic application [30] and modeling of $CH_3NH_3Pb(I_{1-x}Cl_x)_3$ based perovskite solar cell [31]) have been employed to improve the efficiency of heterojunction thin film solar cell by tuning the transport properties [32], changing the deposition or growth conditions [33], engineering the band gap (Cu_2O/Si heterojunction solar cells) [34] or nanostructure interfaces [35], sandwiching the intrinsic or intermediate layers between ZnO/Cu_2O heterojunction to annihilate the defects and enhance the performance of the device [36].

Various processes are available to reduce the defect concentration in Cu_2O TFs for instance annealing or growth in a controlled environment [37,38], by passivation using a cyanide treatment [39] or hydrogen diffusion [40]. The passivation of materials surface/bulk by hydrogen to eliminate defects and improve the electrical and optical properties is well known in the silicon solar cell and semiconductor industry [41,42]. Various techniques are also available to incorporate H^+/H_2 into Cu_2O TFs, e.g. introduction of hydrogen during deposition [43], hydrogen plasma treatment, hydrogen ion implantation [44], and annealing of Cu_2O TFs in hydrogen ambient atmosphere. Hydrogen ions can incorporate and interact with native defects to passivate the acceptor levels through annihilation of the copper vacancy, or by forming O–H bond with the dangling bond of an O atom in the Cu_2O lattice [45]. The impact of hydrogen treatment on polycrystalline nitrogen doped Cu_2O films has previously been investigated to tune the electrical and optical properties, and the hole carrier density was controlled in the range of 10^{16}–10^{18} cm^{-3} [46]. Ishizuka et al. published a comparative study on passivation of defects in polycrystalline nitrogen-doped Cu_2O films by cyanide or hydrogen treatment. The luminescence properties improved while carrier concentration varied from ~10^{16} – 10^{17} cm^{-3} [47]. Ion implantation is a well-known process in semiconductor technology and one of the most reliable techniques for hydrogen ion implantation (also called proton implantation) for passivation of surface/bulk semiconductors. However, low energy ion beam has been used to implant hydrogen ion at room temperature [48].

In the present work, the impact of post annealing temperature in Ar atmosphere and H^+ implantation on structural, surface morphological, electrical and optical properties of annealed Cu_2O TFs have been investigated. The qualitative output acquired by photoluminescence (PL) spectroscopy has been compared with the Hall effect study. A functional correlation is established among Hall effect parameters, post annealing temperature (T_{PA}) and implanted H^+ doses.

2. Experimental method

Cu_2O TFs were deposited by a direct current (DC) magnetron sputtering system (Semicore Triaxis) on 1 x 1 cm^2 quartz substrates in a controlled atmosphere (O_2|Ar ratio) at 400 °C deposition temperature. The pre-sputtering time was 10 min to avoid any contamination. The quartz substrates were cleaned in piranha solution and rinsed in deionized water, blown dry with nitrogen and loaded into the deposition chamber. The deposition power was fixed at 100 W. The base pressure before deposition was below 5×10^{-7} Torr, while the sample stage was rotated at a constant speed of 12 rpm during deposition. The film thickness was determined using ellipsometry (J. A. Woolam alpha - SE) and modeled with the CompleteEASE software and was ~500 nm for all samples. As-grown Cu_2O films were annealed at 900 °C (in an Annealsys Micro rapid thermal annealing (RTA) furnace) for 3 min to improve the structural, optical and electrical properties. After annealing at 900 °C in RTA, the polycrystalline Cu_2O TFs were implanted with various H^+ (Proton) of 5E13, 1E14, 4E14, 1E15 and 2E15 cm^{-2} doses with an implantation energy of 36 keV to passivate the acceptor/defect levels in Cu_2O using a NEC Tandem accelerator at room temperature. The hydrogen ions implantation depth profile was simulated using SRIM code by Ziegler [49]. The X ray diffraction (XRD) pattern was recorded by a Bruker AXS D8 Discover Diffractometer, using Cu K_α-radiation and a Bragg-Brentano configuration. The UV–Vis optical transmittance spectra in the wavelength range from 400 nm to 1500 nm were measured at room temperature using a Shimadzu SolidSpec-3700 DUV spectrophotometer with an integrating sphere. The optical emission properties of TFs were investigated by photoluminescence (PL) measurements at 300 K temperature using a 488 nm Ar cw-laser with an output power of 4.4 mW as the excitation source. The focused laser beam had a power density up to ~20 kW cm^{-2} in a spot of 5 μm diameter on the surface of the samples. The emission was collected by a microscope and directed via a low-pass filter (cut-off wavelength 550 nm) into an imaging spectrometer (Horiba Jobin Yvon, iHR320) coupled with an electron-multiplying CCD camera (Andor, Luca DL-658 M EMCCD) as detector. The system offered a spectral resolution of 0.2 nm. The H^+ implanted (annealed at 900 °C in RTA) Cu_2O TFs were post annealed at 100 °C, 200 °C, 300 °C, 400 °C, 500 °C, and 600 °C in Ar atmosphere. The room temperature as well as temperature dependent Hall effect measurements (LakeShore 7604 set up) using the van-der Pauw method were carried out to determine the hole mobility, resistivity and hole carrier density. The surface morphology measurement was performed on selected samples reported in **Supplementary material (SM)** using scanning electron microscopy (JEOL JSM-IT300 SEM), equipped with a solid state back scattered electrons detector (SS-BSED) and an Everhardt–Thronley secondary electrons (SE) detector. The front surface of Cu_2O TFs was imaged at an acceleration voltage of 20 kV. The surface roughness analysis was performed on selected samples using atomic force microscopy (a Park Systems XE-70 microscope AFM), and has been discussed in detail in **SM**. The instrument is in an anechoic box to reduce background vibrations, and samples are placed onto an anti-vibration holder. The experiments were performed in non-contact mode using a non-contact high-resolution tip from Park Systems. The AFM is controlled by XEP software. The data visualization and analysis were performed using Gwyddion free and open source software [50].

3. Results and discussion

3.1. Structural, optical and microscopic analysis

The XRD pattern of as-deposited Cu_2O TFs, Cu_2O films annealed at 900 °C in RTA and H^+ implanted Cu_2O TFs after annealing in RTA are recorded in the range 30–65° as summarized in Fig. 1. The XRD pattern displays that as–grown polycrystalline Cu_2O TFs is dominated by (111) reflection peak (36.65°) with other reflections peak at (200) and (220) corresponding to 42.61° and 61.34°, respectively. After annealing at 900 °C in RTA, the XRD pattern of annealed Cu_2O TFs show the preferred orientation growth in (200) reflection peak (42.61°) and higher crystallinity [51,52]. The crystallinity of the

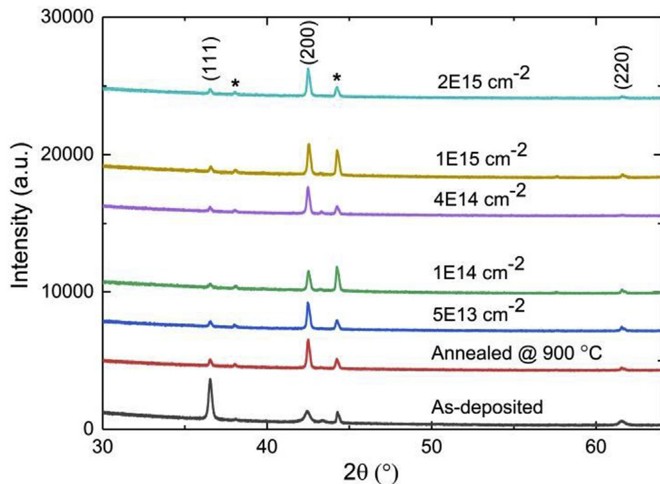

Fig. 1. XRD pattern of as-deposited Cu_2O TF (black line), Cu_2O TF annealed at 900 °C in RTA (red line), and H^+ implanted Cu_2O TFs (color coded) with various H^+ doses (5E13 – 2E15 cm^{-2}) after annealing at 900 °C in RTA. The star (*) indicates the sample holder peak. (For interpretation of the references to colour in this figure legend, the reader is referred to the Web version of this article.)

films improve after annealing as the XRD peak intensity of Cu_2O increased and FWHM (Full Width Half Maximum) decreased because of larger grain sizes **(SM)**. The phase of Cu_2O was determined by comparing the experimental XRD pattern with the Standard Powder Diffraction Cards (ICDD) patterns: 01-071-3645 or space group O_h^4; Pn3m, No. 224 for Cu_2O [53,54]. The peak with star (*) in the XRD pattern belongs to the sample holder as displayed in Fig. 1. Hardly, any effect of H^+ implantation was recorded by XRD on the structural properties of Cu_2O TFs.

3.1.1. Optical band gap and photoluminescence (PL) spectroscopy analysis

The optical band gap of as-deposited, annealed at 900 °C in RTA and H^+ implanted Cu_2O TFs were determined from the transmittance measurements (**SM,** Fig. S1a) using Tauc method, which assumes that absorption coefficient (α) is related to the energy band gap (E_g) by the following equation: $(\alpha\, h\nu) = A(h\nu - E_g)^n$, where A is a constant, $h\nu$ is photon energy and n is an index associated with specific type of optical transition (1/2 direct allowed; 3/2 direct forbidden; 2 indirect allowed; 3 indirect forbidden) [55]. Fig. 2a displays the absorption edge region of spectra plotted as $(\alpha\, h\nu)^2$ versus photon energy ($h\nu$), which infers a linear profile for direct band gap materials. In such Tauc plot, direct optical band gap can be determined from the intercept of the leading edge linear extrapolation with $h\nu$ axis, as displayed by dashed lines in Fig. 2a. The optical band gaps of as-deposited, annealed at 900 °C and H^+ implanted Cu_2O TFs are found to be in the range from ~2.45 to 2.55 eV [56], which agrees well with theoretical and experimental results reported in the literature [57,58]. After annealing at 900 °C in RTA, the films become more transparent and crystalline with larger grain size, all that leading to apparent blue shift of the absorption edge [59]. Next, the transmittance measurements (Fig. S1a) of H^+ implanted and post-annealed Cu_2O TFs were performed to study the impact of variable H^+ doses on the optical properties of TFs. The analysis of transmittance spectra and extracted optical band gaps suggests that Cu_2O TFs were not modified significantly within the applied H^+ dose range, which is in general agreement with the reports in literature [60,61]. This conclusion is also supported by Arita et al. report that hardly any impact on optical properties of copper and aluminum nitride TFs could be recorded after proton implantation [62].

The PL measurements (Fig. S1b) were performed at 300K on post-annealed (900 °C in RTA) and post-implantation annealed (300 °C) Cu_2O TFs subjected to different H^+ doses in order to investigate passivation effects of hydrogen and relaxation mechanisms of localized excitons at optically active defect centers [63]. A qualitative analysis approach has been employed to explain the observed PL spectral developments of the annealed and post-implantation annealed TFs. For this purpose, first the key emission components, excitonic and defect-related, have been designated in spectra, and then corresponding integrated PL intensities were monitored throughout different processing steps (see **SM** for more details). Fig. 2b summarizes PL measurements by presenting H^+ implantation dose dependencies of the integrated PL over three representative regions of spectra - I (excitonic), II (V_O^{++} and V_O^+) and III (V_{Cu}^-) defect-related emissions, respectively.

The pristine (non-implanted) material, represented by post-annealed (Ann 900 °C in RTA) Cu_2O TF exhibits strong excitonic features dominating over negligible defect-related contributions in both regions II and III (Fig. S1b). Upon H^+ implantation, spectral developments in the selected three regions exhibit dissimilar trends with the increase of dose. The defect-related emission in region II (V_O^{++} and V_O^+) increases continuously with increasing H^+ dose (2E13 – 2E15 cm^{-2}), suggesting that the concentration of doubly (V_O^{++}) and singly (V_O^+) ionized oxygen vacancies [64] rises up to two orders of magnitude at high doses (2E15 cm^{-2}) as compared to that of pristine (non-implanted) TFs. The opposite trend is

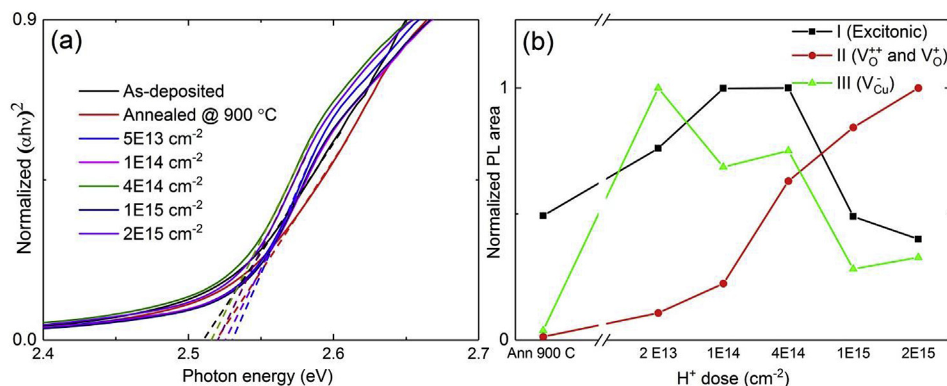

Fig. 2. (a) Optical absorption edge of as deposited (400 °C), post-annealed at 900 °C in RTA and H^+ implanted Cu_2O TFs. The intercepts of linear extrapolations (dashed lines) indicate direct optical band gap energies. (b) Integrated PL intensity as a function of H^+ implantation dose for three representative spectral regions: I (Excitonic), II (V_O^{++} and V_O^+) and III (V_{Cu}^-) defect-related emissions, respectively.

observed for the emission associated with copper vacancy in region III (V_{Cu}^{-}), which appears most prominent (ten-fold increase compared to pristine (non-implanted) TF) after the lowest-dose H^+ implantation (2E13 cm^{-2}) and then decreases steadily with the increase of H^+ dose, presumably as a result of gradual suppression of copper vacancies by hydrogen. Interestingly, these inverse trends of the defect-related emissions II and III versus H^+ dose might explain the local enhancement of excitonic emission (region I) observed at around 1E14 cm^{-2}, which apparently represents the critical point of minimal total density of luminescent defects competing with excitons for a fixed number of the photogenerated carriers. In addition, selected Cu_2O TFs were investigated by SEM and AFM for surface morphology and roughness analysis and have been discussed in detail in the **SM**. No significant difference was observed on surface and morphology of selected samples after post annealing and H^+ implantation (Fig. S5 and Fig. S6).

3.2. Electrical characteristics

3.2.1. Room temperature Hall effect study

Room temperature Hall effect measurement has been performed to investigate the hole mobility, carrier density and resistivity of all Cu_2O TFs. The Hall parameters of as-deposited Cu_2O TF are ~19 cm^2/V, 1.2×10^{15} cm^{-3}, 268 Ωcm and after annealing at 900 °C in RTA, Hall effect parameters changed to ~49 cm^2/V, 5.3×10^{14} cm^{-3}, 627 Ωcm, respectively [65]. Cu_2O is natively cation-deficient and intrinsically “p-type” material due to negatively charged copper vacancies as suggested by first principles theoretical calculation [47]. The H^+ implanted (annealed at 900 °C) TFs and post-implantation annealed (100−600 °C) Cu_2O TFs are also investigated by Hall measurement at room temperature as described in more detail in **SM**. Figs. S2 and S3 present the resistivity, hole mobility, and hole carrier concentrations for all samples. The hole carrier density and mobility have a reciprocal relationship with increasing H^+ doses. The hole mobility increases while carrier density decreases with respect to increasing H^+ doses [66]. The hole mobility is varied in the range of ~ (1−36) cm^2/Vs, while hole carrier density is tuned in the range of 10^{13} - 10^{15} cm^{-3} at different T_{PA} corresponding to various H^+ doses (Figs. S2 and S3). After H^+ incorporation films become more resistive (resistivity varied in between ~ 0.3−5 kΩcm) as compared to as-deposited and annealed TFs [67]. Hence, we found that not only variation of H^+ doses has an impact on functional properties by controlling the hole carrier concentration (copper vacancy), but also that different T_{PA} play a leading role in influencing the electrical properties. This might be because of H^+ diffuses in or out of the Cu_2O TFs or because of trap limited conduction [68] after elevated T_{PA} as discussed in next section.

3.2.2. Impact of H^+ implantation and post-implantation annealing on transport parameters of Cu_2O TFs

Fig. 3 summarized all the results for all H^+ implanted TFs. By employing a quantitative and analytical approach on the conduction mechanism in Cu_2O TFs, a trend is established among Hall parameters when investigating the impact of various H^+ doses and different T_{PA}. Fig. 3a displays the hole carrier density as a function of H^+ doses at elevated T_{PA}. The carrier density reduces as the H^+ dose surges from lower to higher doses. The post implanted TFs exhibit the lowest carrier density at 300 °C. The maximum hole carrier density is recorded ~4.3×10^{15} cm^{-3} at 200 °C T_{PA} for 5E13 cm^{-2}, while minimum carrier density is ~9.5×10^{13} cm^{-3} at 300 °C T_{PA} for 2E15 cm^{-2}. These results, where carrier density reduces with higher H^+ dose reveal that H^+ acts as a copper vacancy restrainer in p-type Cu_2O TFs, presumably which can be a possible reason for the low performance of Cu_2O based heterojunction solar cell [69]. The drop-in carrier density with higher H^+ doses as previously discussed is in a good agreement with Tabuchi et al., where the carrier concentration was controlled by the exposure of atomic hydrogen [70]. Similar outcomes also were found by Ishizuka et al. using Si doping of Cu_2O TFs [71]. In addition, the low temperature post annealing plays a dynamic role to tune the hydrogen diffusion activity by influencing the transport parameters. The present samples are p-type, and the following condition is fulfilled $H_i^+ < V_{Cu}^-$, and most likely H^+ cations will passivate copper vacancy as mentioned in equation (Eq.) 1.

$$H_i^+ + V_{Cu}^- \rightarrow V_{Cu}^0 + H_i^0 \qquad \text{(Eq. 1)}$$

The copper vacancy formation energy is affected by cation substitution such as H^+ in this case. A substitution by a H^+ cation prompts the neutralization of copper vacancies (V_{Cu}^-) by creating the neutral V_{Cu}^0 defect and a subsequent decrease of the hole carrier density, which is likely an indication of passivation of Cu_2O TFs [72].

Fig. 3b displays a relation between T_{PA} after H^+ implantation of annealed Cu_2O TFs versus hole carrier density. The variation in hole carrier density corresponding to various H^+ doses are more visible at elevated T_{PA} (Fig. 3b). The highest hole carrier density is recorded for the lowest dose (5E13 cm^{-2} (black line)) at all T_{PA}. A drop in carrier density is recorded at 300 °C for all H^+ implanted TFs as mentioned in Table 1. This is likely an indication of a favorable hydrogen activation temperature condition. The lowest carrier density is found ~9.5×10^{13} cm^{-3} at 300 °C T_{PA} for 2E15 cm^{-2}.

Fig. 3c and d displays a relation among hole mobility, H^+ doses and T_{PA}. No strong pattern is found in case of hole mobility versus H^+ doses (Fig. 3c). However, hole mobility improves further with higher dose, possibly due to passivation of grain boundaries or copper vacancies. A drastic change in hole mobility is recorded for all H^+ implanted Cu_2O TFs at 300 °C and/or 400 °C T_{PA} (Fig. 3d). The maximum hole mobility is recorded ~36 cm^2/V at 300 °C T_{PA} for 4E14 cm^{-2}, while the lowest hole mobility is recorded ~1 cm^2/V at 200 °C T_{PA} for 5E13 cm^{-2}. The mobility value for the highest H^+ dose 2E15 cm^{-2} is ~27 cm^2/V at 300 °C T_{PA}. In Fig. 3e and f, we investigated the impact of T_{PA} and H^+ implantation on the resistivity of Cu_2O TFs. Fig. 3e shows a variation in resistivity versus H^+ doses and Fig. 3f shows a graph between resistivity versus various T_{PA}. Unclear trend is recorded for resistivity versus H^+ doses. However, the films resistivity changed depending upon the H^+ doping and post annealing temperature. The resistivity is varied from ~0.3−5 kΩcm depending upon T_{PA} and various H^+ doses. The lowest resistivity is recorded ~0.3 kΩcm for 1E14 cm^{-2} at 400 °C (Fig. 3e), while the highest resistivity is obtained ~5 kΩcm for 4E14 cm^{-2} at 100 °C T_{PA} (Fig. 3f).

3.2.3. Temperature dependent Hall measurement (TDH)

The impact of T_{PA} on H^+ implanted and annealed Cu_2O TFs are investigated using TDH by varying the temperature from 180 to 340 K on selected samples post annealed at 300 °C in Ar after H^+ implantation with 1E15 and 2E15 cm^{-2} H^+ dose, respectively. Fig. 4 displays the hole carrier density as a function of temperature. A compensated semiconductor model for a single acceptor level and a single donor level is employed to fit the quantitative behavior of charge carriers following Eq. (2) [73].

$$\frac{p(p+N_d)}{N_a - N_d - p} = \beta N_V \, e^{\frac{-E_a}{kT}} \qquad \text{(Eq. 2)}$$

where p is carrier density, N_a is acceptor concentration, N_d is compensating donor concentration, β is degeneracy level of the acceptor defect (equal to $\frac{1}{4}$), E_a is activation energy level of the defect and N_v is effective density of states of the valence band. The

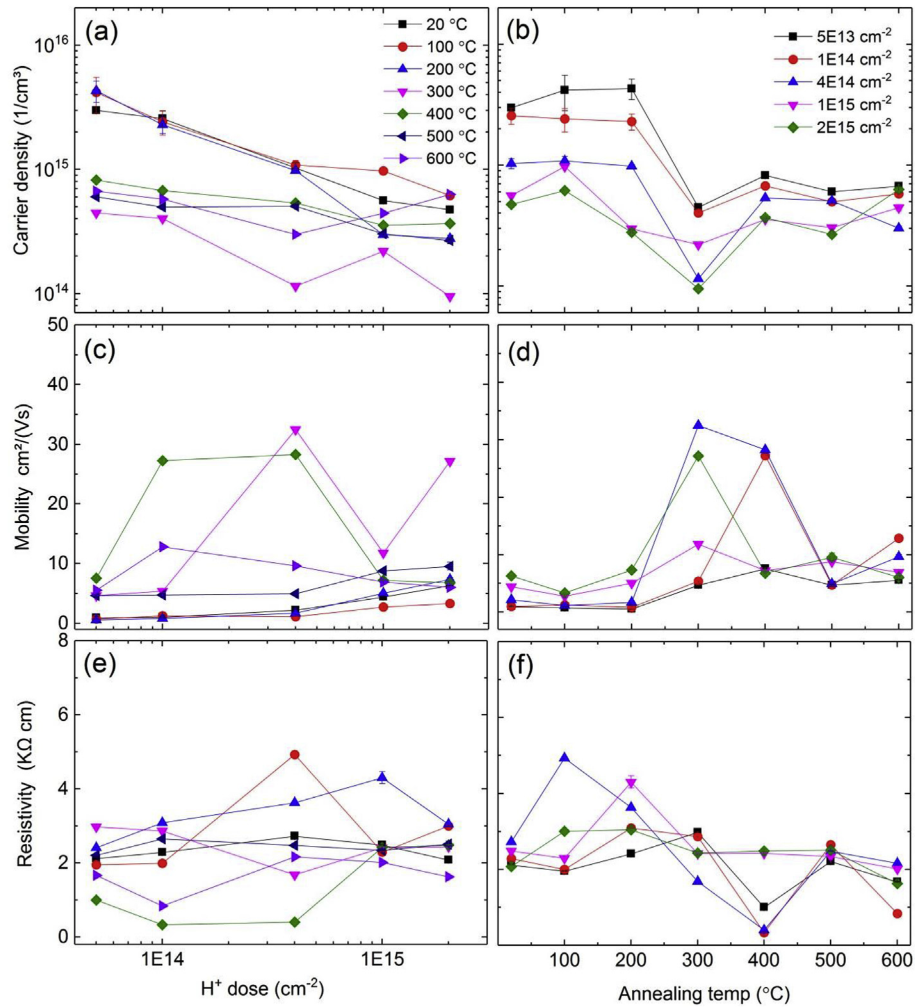

Fig. 3. (a) hole carrier density versus (vs) variation of implanted H^+ dose for annealed, and post annealed Cu_2O TFs after H^+ implantation; (b) hole carrier density vs variation in post annealing temperature (T_{PA}) in Ar for annealed and H^+ implanted Cu_2O TFs; (c) hole mobility vs variation in H^+ doses for annealed and post annealed TFs and (d) hole mobility vs post annealing temperature for annealed and H^+ implanted Cu_2O TFs; (e) resistivity vs various H^+ doses plot for annealed and post annealed TFs, and (f) the resistivity vs post annealing temperatures (T_{PA}) graph for annealed and H^+ implanted Cu_2O TFs.

Table 1
Hole carrier density, mobility and resistivity values of H^+ implanted Cu_2O TFs at 300 °C T_{PA} in Ar atmosphere.

H^+ doses (cm^{-2})	5E13	1E14	4E14	1E15	2E15
Hole carrier density (cm^{-3})	4.5×10^{14}	4.0×10^{14}	1.2×10^{14}	2.2×10^{14}	9.5×10^{13}
Hole mobility (cm^2/VS)	4	9	36	13	27
Resistivity (kΩcm)	3.0	2.8	1.7	2.4	2.4

quantitative fit of the experimental points to Eq. (2) (blue line in Fig. 4) revealed acceptor levels in each case at 0.21 eV (1E15 cm^{-2}) and 0.27 eV (2E15 cm^{-2}) above the VBM (**SM** Fig. S4) and compensation ratio (N_d/N_a) 82% (1E15 cm^{-2}) and 49% (2E15 cm^{-2}), respectively. These results are in good agreement with existing literature on the simple copper vacancies (V_{Cu}^{-}) [74–78]. A theoretical model was published by Scanlon et al. on transition levels for simple copper vacancy (0.23 eV) and split copper vacancy (0.47 eV) in p-type Cu_2O using screened hybrid–density-functional approach to investigate the formation of defect states [79]. Paul et al. studied the experimental value for two trap levels at ~0.25 eV and ~0.45 eV associated to copper vacancy using deep-level transient spectroscopy (DLTS) [70]. Kikuchi et al. also found the ionization energy of the acceptor level to be ~0.22–0.25 eV above the VBM in Cu_2O:Ni [80]. Brochen et al. also studied temperature dependent Hall measurement on Sr doped Cu_2O films. The copper vacancy acceptor level is found at 0.27 eV above the VBM in addition to a coexisting shallow acceptor level with ionization energy about 0.13 eV, which varied with strontium doping [64]. Similarly, a change in acceptor level from 0.21 eV to 0.27 eV is found in this work when H^+ doses varied from 1E15 to 2E15 cm^{-2}, indicating that incorporation of H^+ leads to the acceptor levels moving towards the middle of the band gap.

Concerning the compensation ratio as mentioned in Fig. 4, a reduction in the compensation ratio can be observed by increasing the H^+ dose from 1E15 (82%) to 2E15 (49%) cm^{-2}. The strong reduction of the compensating ratio after annealing at 300 °C with higher H^+ dose (2E15 cm^{-2}) is probably related to a decrease in

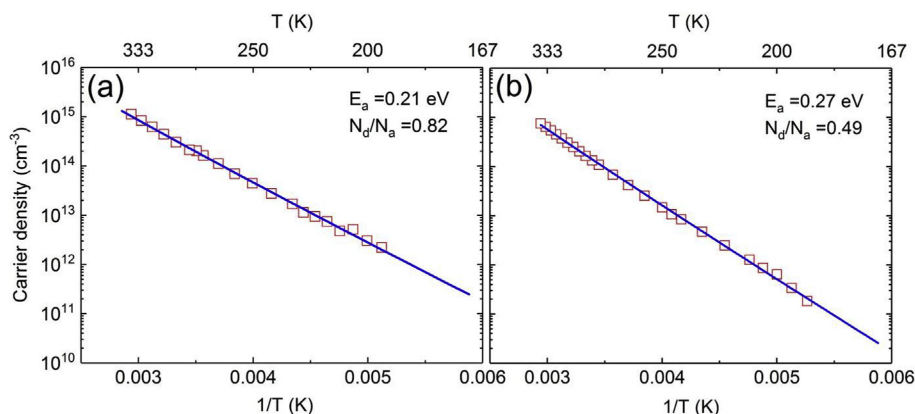

Fig. 4. Temperature dependent Hall Effect measurements of selected samples post annealed at 300 °C in Ar after H^+ implantation, (a) the carrier density as a function of temperature for 1E15 cm^{-2} H^+ dose post annealed at 300 °C in Ar with an ionization energy level at 0.21 eV (blue line); (b) the carrier density as a function of temperature for 2E15 cm^{-2} H^+ dose post annealed at 300 °C in Ar with an ionization energy level at 0.27 eV (blue line) above the VBM. (For interpretation of the references to colour in this figure legend, the reader is referred to the Web version of this article.)

compensating defects due to a passivation in these samples, as reported by Ishizuka et al. [43]. The decrement in compensating ratio might also originate from an increase of the amount of copper vacancies, which is likely to be the most favorable intrinsic acceptors level defect in Cu_2O [47], but the reduction in carrier density with higher hydrogen ion dose (Fig. 3) suggests that the former is dominating in these samples. Hence, H^+ implantation and subsequent annealing leads to a passivation of both acceptor defects and compensating donor defects.

4. Conclusions

The sputtered TFs of polycrystalline Cu_2O show preferential orientation growth after annealing in RTA. Post annealing and H^+ implantation does not show any significant change on structural, optical band gap, surface and morphology of TFs, while the PL spectra and Q. E. yield were tuned subsequently with increasing H^+ dose for all samples. However, the hole carrier density can be controlled by H^+ implantation. The post annealed TFs (300 °C) after H^+ implantation (2E15 cm^{-2}) yielded the lowest hole carrier density of ~9.5×10^{13} cm^{-3}. In addition, the H^+ changes the acceptor level in the Cu_2O films from 0.21 eV to 0.27 eV when the H^+ doping level increased from 1E15 to 2E15 cm^{-2}. The increment in H^+ doses reduce the hole carrier density, indicating that H^+ likely limits the formation of the acceptors level, probably due to the passivation behavior of the H^+ substitution on copper vacancy site. Apparently, the analytical outcomes from PL analysis and Hall measurement culminate that post annealing and H^+ incorporation likely indicate the passivation of both acceptor defects and compensating donor defects. Hence, H^+ passivates both acceptors and donors in Cu_2O TFs.

Author contributions

Raj Kumar: DoE, experiment, methodology, original manuscripts writing, data analysis, Kristin Bergum: Reviewing, AFM measurement and editing manuscripts, discussion, Heine Nygard Riise: Electrical THD measurement, reviewing and editing manuscripts, discussion, Eduard Monakhov: Supervision, reviewing and editing manuscripts, discussion, project managing, Augustinas Galeckas: PL measurement, PL data analysis, reviewing and editing manuscripts, discussion.

Declaration of competing interest

There is no conflict of interest in this article.
Funding resources has been included.
All authors has read and approved the manuscripts.
These is no ethical and IPR issue in this manuscripts.

Acknowledgements

This work was conducted under the research project "High-performance tandem hetero-junction solar cells for specific applications (SOLHET) http://solhet.eu/," financially supported by the Research Council of Norway (RCN) and the Executive Agency for Higher Education, Research Development and Innovation Funding (UEFISCDI) through the EU-H2020 M-Era.net program. The Research Council of Norway is acknowledged for the support to the Norwegian Micro- and Nano-Fabrication Facility, NorFab, project number 245963/F50. I would like to thank Mr. Viktor bobal for ion implantation and technical support during the experiment.

Appendix A. Supplementary data

Supplementary data to this article can be found online at https://doi.org/10.1016/j.jallcom.2020.153982.

References

[1] P. Cendula, M.T. Mayer, J. Luo, M. Grätzel, Elucidation of photovoltage origin and charge transport in Cu2O heterojunctions for solar energy conversion, Sustain. Energy Fuels 3 (2019) 2633–2641.
[2] C. Qin, Y. Wang, Z. Lou, S. Yue, W. Niu, L. Zhu, Surface modification and stoichiometry control of Cu2O/SnO2 heterojunction solar cell by an ultrathin MgO tunneling layer, J. Alloys Compd. 779 (2019) 387–393.
[3] T.K. Wong, S. Zhuk, S. Masudy-Panah, G.K. Dalapati, Current status and future prospects of copper oxide heterojunction solar cells, Materials 9 (2016) 271.
[4] D.-C. Perng, M.-H. Hong, K.-H. Chen, K.-H. Chen, Enhancement of short-circuit current density in Cu2O/ZnO heterojunction solar cells, J. Alloys Compd. 695 (2017) 549–554.
[5] Y. Takiguchi, S. Miyajima, Device simulation of cuprous oxide heterojunction solar cells, Jpn. J. Appl. Phys. 54 (2015) 112303.
[6] Z. Starowicz, K. Gawlińska-Nęcek, M. Bartmański, M. Wlazło, T. Płociński, B. Adamczyk-Cieślak, G. Putynkowski, P. Panek, Investigation of the Zn and Cu oxides for heterojunction thin film solar cell application, Microelectron. Eng. 221 (2020) 111196.
[7] H. Al-Jawhari, A review of recent advances in transparent p-type Cu2O-based thin film transistors,, Mater. Sci. Semicond. Process. 40 (2015) 241–252.
[8] J.-S. Yoon, J.-W. Lee, Y.-M. Sung, Enhanced photoelectrochemical properties of Z-scheme ZnO/pn Cu2O PV-PEC cells, J. Alloys Compd. 771 (2019) 869–876.
[9] T. Li, M. He, W. Zeng, Polyhedral Cu2O crystal: morphology evolution from

meshed nanocube to solid and gas-sensing performance, J. Alloys Compd. 712 (2017) 50–58.
[10] S.B. Nacer, D. Jlidi, A. Labidi, F.C. Akkari, S. Touihri, M. Maaref, Promising ethanol detection enhancement of Cu2O thin film deposited by GLAD technique, Measurement 151 (2020) 107208.
[11] N. Khaliq, M.A. Rasheed, G. Cha, M. Khan, S. Karim, P. Schmuki, G. Ali, Development of non-enzymatic cholesterol bio-sensor based on TiO2 nanotubes decorated with Cu2O nanoparticles, Sensor. Actuator. B Chem. 302 (2020) 127200.
[12] Y. Wang, A. Steigert, G. Yin, V. Parvan, R. Klenk, R. Schlatmann, I. Lauermann, Cu2O as a potential intermediate transparent conducting oxide layer for monolithic perovskite-CIGSe tandem solar cells, Phys. Status Solidi C 14 (2017) 1700164.
[13] S. Fu, J. Chen, H. Han, W. Wang, H. Shi, J. Fu, Y. Jia, ZnO@ Au@ Cu2O nanotube arrays as efficient visible-light-driven photoelectrod, J. Alloys Compd. 799 (2019) 183–192.
[14] J. Pan, S. Li, Y. Liu, W. Ou, H. Li, W. Zhao, J. Wang, C. Song, Y. Zheng, C. Li, The flexible-transparent pn junction film device of N-doped Cu2O/SnO2 orderly nanowire arrays towards highly photovoltaic conversion and stability, Chem. Eng. J. 382 (2020) 122813.
[15] Z. Zang, Efficiency enhancement of ZnO/Cu2O solar cells with well oriented and micrometer grain sized Cu2O films, Appl. Phys. Lett. 112 (2018), 042106.
[16] H. Wei, H. Gong, Y. Wang, X. Hu, L. Chen, H. Xu, P. Liu, B. Cao, Three kinds of Cu 2 O/ZnO heterostructure solar cells fabricated with electrochemical deposition and their structure-related photovoltaic properties, CrystEngComm 13 (2011) 6065–6070.
[17] H. Wei, H. Gong, L. Chen, M. Zi, B. Cao, Photovoltaic efficiency enhancement of Cu2O solar cells achieved by controlling homojunction orientation and surface microstructure, J. Phys. Chem. C 116 (2012) 10510–10515.
[18] Ø. Nordseth, R. Kumar, K. Bergum, L. Fara, S.E. Foss, H. Haug, F. Drăgan, D. Crăciunescu, P. Sterian, I. Chilibon, Optical analysis of a ZnO/Cu2O subcell in a silicon-based tandem heterojunction solar cell, Green Sustain. Chem. 7 (2017) 57–69.
[19] Z. Luo, L. Fu, J. Zhu, W. Yang, D. Li, L. Zhou, Cu2O as a promising cathode with high specific capacity for thermal battery, J. Power Sources 448 (2020) 227569.
[20] S. Kallatt, S. Nair, K. Majumdar, Asymmetrically encapsulated vertical ITO/MoS2/Cu2O photodetector with ultrahigh sensitivity, Small 14 (2018) 1702066.
[21] R. Chakraborty, H. Bhunia, S. Chatterjee, A.J. Pal, Surface-modification of Cu2O nanoparticles towards band-optimized hole-injection layers in CsPbBr3 perovskite light-emitting diodes, J. Solid State Chem. 281 (2020) 121021.
[22] J. Luo, L. Steier, M.-K. Son, M. Schreier, M.T. Mayer, M. Grätzel, Cu2O nanowire photocathodes for efficient and durable solar water splitting, Nano Lett. 16 (2016) 1848–1857.
[23] C.-L. Kuo, R.-C. Wang, J.-L. Huang, C.-P. Liu, C.-K. Wang, S.-P. Chang, W.-H. Chu, C.-H. Wang, C.-h. Tu, The synthesis and electrical characterization of Cu2O/Al: ZnO radial p–n junction nanowire arrays, Nanotechnology 20 (2009) 365603.
[24] T.P. White, N.N. Lal, K.R. Catchpole, Tandem solar cells based on high-efficiency c-Si bottom cells: top cell requirements for> 30% efficiency, IEEE J. Photovolt. 4 (2013) 208–214.
[25] T. Minami, Y. Nishi, T. Miyata, Efficiency enhancement using a Zn1− x Ge x-O thin film as an n-type window layer in Cu2O-based heterojunction solar cells, APEX 9 (2016), 052301.
[26] T.T. Ly, T. Lee, S. Kim, Y.J. Lee, G. Duvjir, K. Jang, K. Palotás, S.Y. Jeong, A. Soon, J. Kim, Growing ultrathin Cu2O films on highly crystalline Cu (111): a closer inspection from microscopy and theory, J. Phys. Chem. C 123 (2019) 12716–12721.
[27] R. Kara, H. Lahmar, L. Mentar, R. Siab, F. Kadirgan, A. Azizi, Electrochemical growth and characterization of Cu2O: Na/ZnO heterojunctions for solar cells applications, J. Alloys Compd. (2019) 152748.
[28] D. Osorio-Rivera, G. Torres-Delgado, R. Castanedo-Pérez, J. Márquez-Marín, O. Zelaya-Ángel, Cd2SnO4/CdS/Cu2O/Ag solar cell obtained by chemical techniques, Mater. Res. Bull. 122 (2020) 110669.
[29] H. Yin, Y. Zhao, J. Li, Q. Yang, W. Wu, Optical and electrical properties of Ag: Cu2O nanocomposite films prepared by pulse laser deposition, Mater. Chem. Phys. 241 (2020) 122399.
[30] L. Lin, L. Jiang, P. Li, B. Fan, Y. Qiu, A modeled perovskite solar cell structure with a Cu2O hole-transporting layer enabling over 20% efficiency by low-cost low-temperature processing, J. Phys. Chem. Solid. 124 (2019) 205–211.
[31] S. Rai, B. Pandey, D. Dwivedi, Modeling of highly efficient and low cost CH3NH3Pb (I1-xClx) 3 based perovskite solar cell by numerical simulation, Opt. Mater. 100 (2020) 109631.
[32] R. Yatskiv, S. Tiagulskyi, J. Grym, J. Vaniš, N. Bašinová, P. Horak, A. Torrisi, G. Ceccio, J. Vacik, M. Vrňata, Optical and electrical characterization of CuO/ZnO heterojunctions, Thin Solid Films 693 (2020) 137656.
[33] T. Miyata, K. Watanabe, H. Tokunaga, T. Minami, Photovoltaic properties of Cu2O-based heterojunction solar cells using n-type oxide semiconductor nano thin films prepared by low damage magnetron sputtering method, J. Semiconduct. 40 (2019), 032701.
[34] Y. Liu, J. Zhu, L. Cai, Z. Yao, C. Duan, Z. Zhao, C. Zhao, W. Mai, Solution-processed high-quality Cu2O thin films as hole transport layers for pushing the conversion efficiency limit of Cu2O/Si heterojunction solar cells, Sol. RRL (2019) 1900339.
[35] S.Z. Haider, H. Anwar, Y. Jamil, M. Shahid, A comparative study of interface engineering with different hole transport materials for high-performance perovskite solar cells, J. Phys. Chem. Solid. 136 (2020) 109147.
[36] A. Boughelout, R. Macaluso, I. Crupi, B. Megna, M. Aida, M. Kechouane, Improved Cu 2 O/AZO heterojunction by inserting a thin ZnO interlayer grown by pulsed laser deposition, J. Electron. Mater. (2019) 1–8.
[37] T. Ha, I. Park, K.I. Sim, H. Lee, J.-S. Bae, S.J. Kim, J.P. Kim, T.-T. Kim, J.H. Kim, J.I. Jang, S.-Y. Jeong, Single-crystalline Cu2O thin films of optical quality as obtained by the oxidation of single-crystal Cu thin films at low temperature, Apl. Mater. 7 (2019), 031115.
[38] D. Ozaslan, O. Erken, M. Gunes, C. Gumus, The effect of annealing temperature on the physical properties of Cu2O thin film deposited by SILAR method, Phys. B Condens. Matter 580 (2020) 411922.
[39] H. Kobayashi, A. Asano, M. Takahashi, K. Yoneda, Y. Todokoro, Decrease in gap states at ultrathin SiO 2/Si interfaces by crown-ether cyanide treatment, Appl. Phys. Lett. 77 (2000) 4392–4394.
[40] R. Rizk, P. De Mierry, D. Ballutaud, M. Aucouturier, D. Mathiot, Hydrogen diffusion and passivation processes in p-and n-type crystalline silicon, Phys. Rev. B 44 (1991) 6141.
[41] H. Yagi, K. Matsukuma, S. Kokunai, Y. Kida, N. Kawakami, K. Nishinoiri, T. Saitoh, R. Shimokawa, K. Morita, Hydrogen passivation of large-area poly-crystalline silicon solar cells by high-current ion implantation, in: Conf. Rec. Twent. IEEE Photovolt. Spec. Conf., IEEE, 1988, pp. 1600–1603.
[42] N. Sieber, B. Mantel, T. Seyller, J. Ristein, L. Ley, T. Heller, D.R. Batchelor, D. Schmeißer, Electronic and chemical passivation of hexagonal 6H–SiC surfaces by hydrogen termination, Appl. Phys. Lett. 78 (2001) 1216–1218.
[43] K. Hering, C. Kandzia, J. Benz, B. Kramm, M. Eickhoff, P. Klar, Hydrogen induced mobility enhancement in RF sputtered Cu2O thin films, J. Appl. Phys. 120 (2016) 185705.
[44] J. Chevallier, M. Aucouturier, Hydrogen in crystalline semiconductors, Annu. Rev. Mater. Sci. 18 (1988) 219–256.
[45] J.Y. Kim, J.A. Rodriguez, J.C. Hanson, A.I. Frenkel, P.L. Lee, Reduction of CuO and Cu2O with H2: H embedding and kinetic effects in the formation of suboxides, J. Am. Chem. Soc. 125 (2003) 10684–10692.
[46] S. Ishizuka, S. Kato, Y. Okamoto, K. Akimoto, Hydrogen treatment for poly-crystalline nitrogen-doped Cu2O thin film, J. Cryst. Growth 237 (2002) 616–620.
[47] S. Ishizuka, S. Kato, Y. Okamoto, T. Sakurai, K. Akimoto, N. Fujiwara, H. Kobayashi, Passivation of defects in polycrystalline Cu2O thin films by hydrogen or cyanide treatment, Appl. Surf. Sci. 216 (2003) 94–97.
[48] J.C. Barbour, J.W. Braithwaite, A.F. Wright, Determination of solid-state sulfidation mechanisms in ion-implanted copper, nucl. Instruments methods phys. Res. Sect. B beam interact. With mater, Atoms 175 (2001) 382–387.
[49] J.F. Ziegler, M.D. Ziegler, J.P. Biersack, SRIM–The stopping and range of ions in matter (2010), Nucl. Instrum. Methods Phys. Res. Sect. B Beam Interact. Mater. Atoms 268 (2010) 1818–1823.
[50] http://gwyddion.net.
[51] J. Hsieh, P. Kuo, K. Peng, S.-J. Liu, J. Hsueh, S. Chang, Opto-electronic properties of sputter-deposited Cu2O films treated with rapid thermal annealing, Thin Solid Films 516 (2008) 5449–5453.
[52] S.W. Lee, Y.S. Lee, J. Heo, S.C. Siah, D. Chua, R.E. Brandt, S.B. Kim, J.P. Mailoa, T. Buonassisi, R.G. Gordon, Improved Cu2O-based solar cells using atomic layer deposition to control the Cu oxidation state at the p-n junction, Adv. Energy Mater. 4 (2014) 1301916.
[53] J. Gan, V. Venkatachalapathy, B. Svensson, E. Monakhov, Influence of target power on properties of CuxO thin films prepared by reactive radio frequency magnetron sputtering, Thin Solid Films 594 (2015) 250–255.
[54] H. Raebiger, S. Lany, A. Zunger, Origins of the p-type nature and cation deficiency in Cu 2 O and related materials, Phys. Rev. B 76 (2007), 045209.
[55] J. Tauc, R. Grigorovici, A. Vancu, Optical properties and electronic structure of amorphous germanium, Phys. Status Solidi 15 (1966) 627–637.
[56] X. Liu, M. Xu, X. Zhang, W. Wang, X. Feng, A. Song, Pulsed-laser-deposited, single-crystalline Cu2O films with low resistivity achieved through manipulating the oxygen pressure, Appl. Surf. Sci. 435 (2018) 305–311.
[57] C. Malerba, F. Biccari, C.L.A. Ricardo, M. D'Incau, P. Scardi, A. Mittiga, Absorption coefficient of bulk and thin film Cu2O, Sol. Energy Mater. Sol. Cells 95 (2011) 2848–2854.
[58] N. Soundaram, R. Chandramohan, R.D. Prabu, S. Valanarasu, K. Jeyadheepan, A. Kathalingam, M.S. Hamdy, A.M. Alhanash, K. Al-Namshah, Preparation of Eu-doped Cu 2 O thin films using different concentrations by SILAR and their heterojunction property with ZnO, J. Electron. Mater. 48 (2019) 4138–4147.
[59] L. Ai, G. Fang, L. Yuan, N. Liu, M. Wang, C. Li, Q. Zhang, J. Li, X. Zhao, Influence of substrate temperature on electrical and optical properties of p-type semi-transparent conductive nickel oxide thin films deposited by radio frequency sputtering, Appl. Surf. Sci. 254 (2008) 2401–2405.
[60] R. Sethi, P. Kumar, S.A. Khan, A. Aziz, A.M. Siddiqui, Effect of nitrogen ion implantation on the structural and optical properties of indium oxide thin films, in: AIP Conf. Proc., AIP Publishing, 2016, 030016.
[61] T. Ishikawa, M. Masuda, Y. Hayashi, Hydrogen implantation effects on the electrical and optical properties of metal nitride thin films, Mater. Trans. 43 (2002) 1138–1141.
[62] M. Arita, H. Konishi, M. Masuda, Y. Hayashi, Effects of protium introduction on electrical and optical properties of tin-germanium oxide thin films, Mater. Trans. 43 (2002) 2670–2672.
[63] D. Snoke, A. Shields, M. Cardona, Phonon-absorption recombination luminescence of room-temperature excitons in Cu 2 O, Phys. Rev. B 45 (1992)

11693.
[64] T. Ito, T. Masumi, Detailed examination of relaxation processes of excitons in photoluminescence spectra of Cu 2 O, J. Phys. Soc. Jpn. 66 (1997) 2185–2193.
[65] K. Bergum, H.N. Riise, S. Gorantla, P.F. Lindberg, I.J. Jensen, A.E. Gunnæs, A. Galeckas, S. Diplas, B.G. Svensson, E. Monakhov, Improving carrier transport in Cu2O thin films by rapid thermal annealing, J. Phys. Condens. Matter 30 (2018), 075702.
[66] S. Kohiki, M. Nishitani, T. Wada, T. Hirao, Enhanced conductivity of zinc oxide thin films by ion implantation of hydrogen atoms, Appl. Phys. Lett. 64 (1994) 2876–2878.
[67] Y. Shigesato, D.C. Paine, T. Haynes, Study of the effect of ion implantation on the electrical and microstructural properties of tin-doped indium oxide thin films, J. Appl. Phys. 73 (1993) 3805–3811.
[68] S. Han, A.J. Flewitt, Analysis of the conduction mechanism and copper vacancy density in p-type Cu 2 O thin films, Sci. Rep. 7 (2017) 5766.
[69] D.O. Scanlon, G.W. Watson, Uncovering the complex behavior of hydrogen in Cu 2 O, Phys. Rev. Lett. 106 (2011) 186403.
[70] N. Tabuchi, H. Matsumura, Control of carrier concentration in thin cuprous oxide Cu2O films by atomic hydrogen, Jpn. J. Appl. Phys. 41 (2002) 5060.
[71] S. Ishizuka, S. Kato, Y. Okamoto, K. Akimoto, Control of hole carrier density of polycrystalline Cu 2 O thin films by Si doping, Appl. Phys. Lett. 80 (2002) 950–952.
[72] S.p. Brochen, L. Bergerot, W. Favre, J.o. Resende, C. Jiménez, J.-L. Deschanvres, V. Consonni, Effect of strontium incorporation on the p-type conductivity of Cu2O thin films deposited by metal–organic chemical vapor deposition, J. Phys. Chem. C 120 (2016) 17261–17267.
[73] P. Blood, J.W. Orton, The Electrical Characterization of Semiconductors: Majority Carriers and Electron States, Academic press London, 1992.
[74] G. Paul, R. Ghosh, S. Bera, S. Bandyopadhyay, T. Sakurai, K. Akimoto, Deep level transient spectroscopy of cyanide treated polycrystalline p-Cu2O/n-ZnO solar cell, Chem. Phys. Lett. 463 (2008) 117–120.
[75] G. Paul, Y. Nawa, H. Sato, T. Sakurai, K. Akimoto, Defects in Cu 2 O studied by deep level transient spectroscopy, Appl. Phys. Lett. 88 (2006) 141901.
[76] K. Matsuzaki, K. Nomura, H. Yanagi, T. Kamiya, M. Hirano, H. Hosono, Epitaxial growth of high mobility Cu 2 O thin films and application to p-channel thin film transistor, Appl. Phys. Lett. 93 (2008) 202107.
[77] Y.S. Lee, M.T. Winkler, S.C. Siah, R. Brandt, T. Buonassisi, Hall mobility of cuprous oxide thin films deposited by reactive direct-current magnetron sputtering, Appl. Phys. Lett. 98 (2011) 192115.
[78] S. Ishizuka, S. Kato, T. Maruyama, K. Akimoto, Nitrogen doping into Cu2O thin films deposited by reactive radio-frequency magnetron sputtering, Jpn. J. Appl. Phys. 40 (2001) 2765.
[79] D.O. Scanlon, B.J. Morgan, G.W. Watson, A. Walsh, Acceptor levels in p-type Cu 2 O: rationalizing theory and experiment, Phys. Rev. Lett. 103 (2009), 096405.
[80] N. Kikuchi, K. Tonooka, E. Kusano, Mechanisms of carrier generation and transport in Ni-doped Cu2O, Vacuum 80 (2006) 756–760.